Hindawi
Shock and Vibration
Volume 2023, Article ID 6667171, 12 pages
https://doi.org/10.1155/2023/6667171

Research Article

Vulnerability Analysis of Catenary-Bridge-Track System

Bin Yan,[1] Limei Yu,[1] Zhe Li,[2] and Zhiping Zeng [1]

[1]*School of Civil Engineering, Central South University, Changsha, Hunan 410075, China*
[2]*Zhengzhou Railway Construction Management Co., Ltd., Zhengzhou, Henan 450006, China*

Correspondence should be addressed to Zhiping Zeng; csu_2022@163.com

Received 28 March 2023; Revised 10 August 2023; Accepted 18 August 2023; Published 29 August 2023

Academic Editor: Antonio Batista

Continuous welded rails on bridges are extensively employed in high-speed railways, where trains are predominantly electrically powered, and the open-air catenary represents the weakest link in the system. Despite the widespread use of continuous welded rail on bridges for high-speed railways, there exists a relative dearth of research on their vulnerability, particularly regarding seismic vulnerability studies that consider the catenary, track type, and bridge collectively. The vulnerability of fasteners and catenary on bridges under the longitudinal resistance of the line was investigated by constructing a 7–32 m high-speed railway double-line simply-supported box girder bridge. It reveals, for the first time, the influence of the longitudinal resistance of the line on the vulnerability of fasteners and catenary under seismic action. The study indicates that both the fasteners' and catenary's vulnerability increases with the intensity of ground shaking, with the catenary being more susceptible. The longitudinal resistance of the line has a greater impact on the fasteners' vulnerability than the catenary. When the degree of damage is minimal, the order of damage to the fasteners is the ballasted track, small resistance fastener, and ballastless track when the probability of exceedance is 5%. The ballastless track can significantly increase the probability of no damage to the fasteners, and it is recommended that the ballastless track be used when designing high-speed railway bridges in earthquake-prone regions.

1. Introduction

With the swift progression of high-speed rail in China, the utilization of continuous welded rail structures on bridges is becoming increasingly prevalent [1]. Generally, China's railway trains apply an electric traction system. According to the 2021 railway statistical bulletin, the national railway electrification proportion in China has now reached 75.4%. The electric traction system is a pivotal component of the electrified railway, which comprises of catenary, pantograph, traction substation, and other technical apparatus, with the catenary being the frailest link as it is right open and has no backup due to external environmental factors [2].

China's geographical location is quite unique, making it particularly vulnerable to frequent earthquake disasters. About half of the existing high-speed railway systems are located within the North China earthquake zone, an area renowned for its high earthquake intensity and frequency. Furthermore, these railway systems have been steadily extended to more seismically active zones such as the Qinghai-Tibet Plateau and the southeast coastal seismic zone. Consequently, earthquake actively endangers the safe operation of trains, making practitioners attach the utmost importance to researching the seismic performance of continuous welded rail bridges. As such, performance-based seismic designs have increasingly gained traction, with seismic vulnerability analysis being pivotal to the design process, looking to offer immense value to seismic designs and seismic performance evaluations.

Scholars have largely focused their research on the vulnerability of highway bridges, with only limited attention being focused on that of high-speed railway bridges. For instance, Tavares et al. [3] employed the Monte Carlo method to quantify the seismic vulnerability of highway bridges; Yang et al. [4] evaluated the seismic performance of different bridge types according to their respective vulnerability curves; Siqueira et al. [5] studied the influence of seismic isolation devices on piers and foundations by

plotting their vulnerability curves; and Li-feng et al. [6] proposed a seismic vulnerability analysis approach based on classical reliability theory, which was then applied to examine the seismic performance of medium multispan concrete continuous girder bridges. Yang et al. [7] examined the effect of pier height on the vulnerability of a simply-supported girder bridge based on the 32 m simply-supported girder bridge along the Sichuan-Tibet railway line. Song et al. [8] utilized the Copula function to formulate the vulnerability curve of the continuous girder bridge bearings and piers of high-speed railways, and proposed a vulnerability analysis method for bridge systems considering the correlation of seismic demands of components. In addition, Dong et al. [9] studied the vulnerability of bridge piers and supports under three-dimensional earthquake action, taking high-pier and long-span railway bridges as the research object.

Regarding the research on the dynamic performance of catenary, there has been some progress. For instance, Kim et al. [10] investigated the impact of catenary spacing on its seismic response by constructing a finite element model of the catenary system. Gregori et al. [11] studied the dynamic performance of high-speed railway overlapping catenary systems, considering double cantilevers and tensioning devices, with numerical simulations. Liu et al. [12] examined the influence of train speed on catenary fatigue and safety reliability based on dynamic stress test data and two-dimensional finite element simulation data of the Re250−0 simple chain suspension catenary. Zhang and Xie [13] investigated the influence of different connection forms and contact line tension on the seismic response of the structure through a four-column three-span finite element model of catenary.

At present, there is a relative lack of studies on the vulnerability of continuous welded rail on high-speed railway bridges, especially those that consider the catenary, track type, and bridge structure when assessing their seismic vulnerability.

To explore the influence of line longitudinal resistance on the vulnerability of the catenary-bridge-track system, this paper takes a 7−32 m double-line simply-supported box girder bridge and establishes a finite element simulation model, which includes catenary pillar (including wrist arm structure), track structure (ballasted track, ballastless track, and small resistance fastener), and bridge structure. It reveals the seismic vulnerability of each component of the system and discusses the influence of the longitudinal resistance of the line on the vulnerability of the fasteners and catenary. The response patterns of the components under seismic motion are also analyzed.

2. Simulation Model of the Catenary-Bridge-Track System

2.1. Simulation of System Structure. In this paper, a simulation model for the catenary-bridge-track system is primarily established, which takes into account various structures such as the catenary, steel rail, fastener, beam, support, bridge pier, and bridge abutment, among others.

Considering that the contact line is prone to significant elastic deformation and failure during strong earthquakes, for the sake of simplification, this study focused on modeling the catenary pillar and wrist arm system as research objects [14]. To achieve this, all components of the catenary pillar and wrist arm system were simulated using frame units. The section form of the catenary pillar adopts H-shaped steel column of GH240 model, and its section size is shown in Figure 1(a). It is made of Q235 with a column height of 7.5 m. Meanwhile, the wrist arm system was comprised of a wrist arm support device and a positioner, with the support device selected as the seamless steel tube wrist arm support device (WG type) and the positioner as the limit positioning device. Insulators were used to connect the wrist arm support device and the catenary column. The relative positions of each component are depicted in Figure 1(b), while the specific parameters can be found in Table 1. To establish the catenary, the study started from the 1/4 span of the leftmost span of the simply-supported beam, with the catenary being established 50 meters apart from left to right and numbered as 1#, 2#, ... 5#.

The steel rail utilized in this study was the CHN60 rail, with Q345 material being selected and simulated using the frame unit. Meanwhile, the fastener was simulated using the nonlinear connection unit, taking into account the resistance in the three-dimensional direction. The relationship between the resistance and displacement was determined using formulas (1)–(3) [15]:

$$r_{L_1}\begin{cases} 12x, & |x| \le 2, \\ 24\mathrm{sign}(x), & |x| > 2, \end{cases} \tag{1}$$

where r_{L_1} is the longitudinal resistance of the fastener, kN/m per line, and x is the longitudinal relative displacement between the rail and the rail bearing platform, mm.

$$r_T\begin{cases} 4.5y, & |y| \le 2, \\ 9\mathrm{sign}(y), & |y| > 2, \end{cases} \tag{2}$$

where r_T is the lateral resistance of the fastener, kN/m per line, and y is the lateral relative displacement between the rail and the rail bearing platform, mm.

$$r_V\begin{cases} 23z - 18, & -10 \le z < -9, \\ 25z, & -9 \le z < 0, \\ 25.09z, & 0 \le z < 0.78, \\ 2z + 18.01, & 0.78 \le z < 1.78, \end{cases} \tag{3}$$

where r_V is the vertical resistance of the fastener, kN/m per line, and z is the vertical relative displacement between the rail and the rail bearing platform, mm.

To mitigate boundary conditions, a 200 m track was established at each end of the bridge span structure [16], with the fastener connection unit being linked to the subgrade.

The beam was a 7−32 m double-line prestressed equal-section simply-supported box girder with C55 concrete and a cross-sectional area of 9.2826 m^2. The concrete density is 2250 kg/m^3, the elastic modulus is 36 GPa, and the Poisson ratio is 0.2, whose cross-sectional is shown in Figure 2. It was

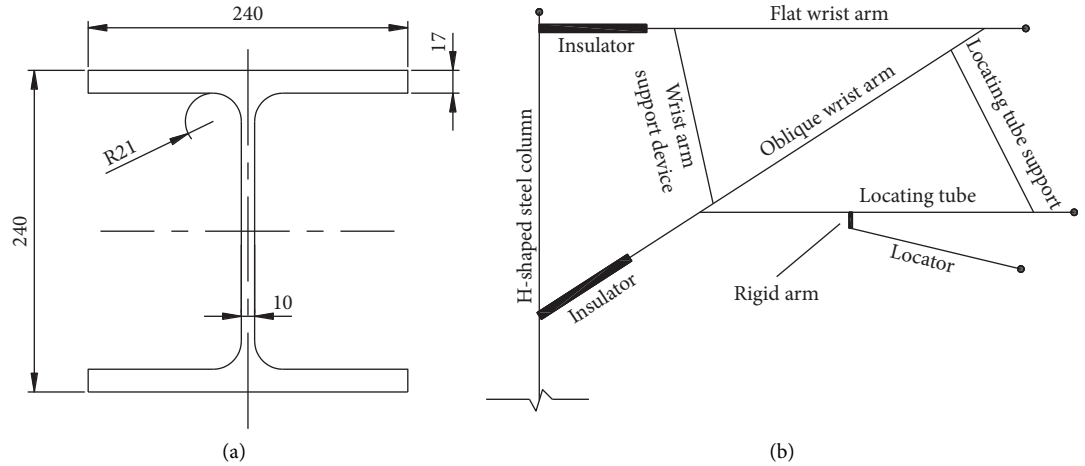

Figure 1: Schematic diagram of the wrist arm system. (a) Section dimensions of H-shaped steel column (unit: mm). (b) The structure of the wrist arm system.

Table 1: Component parameters of the wrist arm system.

Components	Material	Cross-sectional form	Section size (mm)	Length (m)
Flat wrist arm	20#steel	Seamless steel tube	$\Phi 60 \times 5.0$	2.385
Oblique wrist arm	20#steel	Seamless steel tube	$\Phi 60 \times 5.0$	2.654
Wrist arm support device	20#steel	Seamless steel tube	$\Phi 48 \times 3.5$	1.124
Locating tube	20#steel	Seamless steel tube	$\Phi 48 \times 3.5$	2.355
Locating tube support	20#steel	Seamless steel tube	$\Phi 34 \times 2.5$	1.141
Locator	608 aluminium alloy	Rectangular tube	$41 \times 21 \times 3$	1.100
Insulator	Composite ceramic	Solid cylinder	$\Phi 110$	6.750

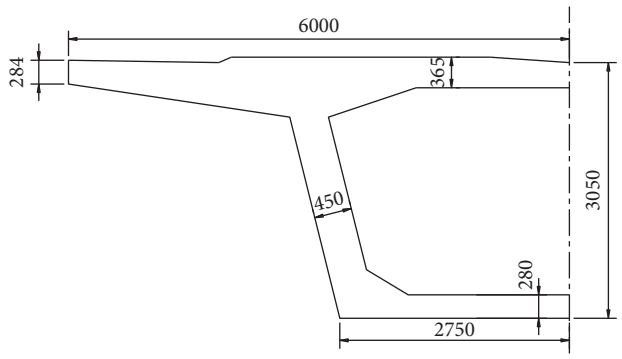

Figure 2: Schematic diagram of beam section (unit: mm).

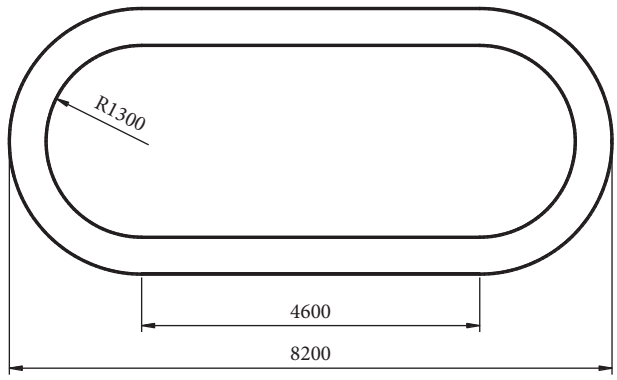

Figure 3: Pier cross-sectional diagram (unit: mm).

simulated using frame units, whose secondary constant loads were considered in the modeling. The fixed support was modeled using the linear connection element Linear, while the sliding support was based on the ideal elastic-plastic spring model. The cut off point of elastoplastic deformation was set at 3 mm, with a friction coefficient of 0.3 [17].

The bridge pier had a hollow thin-walled structure with circular ends, standing at a height of 20 m with a wall thickness of 0.5 m, and made of C40 concrete. The cross-sectional dimensions are shown in Figure 3. The Mander confined model was employed for simulation, taking into account the constraints imposed by stirrups. The cross-sectional moment-curvature curve can be observed in Figure 4. The interaction between the pile group foundation and the soil was simplified as a stiffness matrix with 6 degrees of freedom and was simulated using the linear connection element Linear. At both ends of the bridge, the abutments were round-ended solid pier structures with a height of 4 meters, and both the piers and abutments were simulated using frame units.

The key to establishing a simulation model for the catenary-bridge-track system lies in simulating the contact mode between the bridge, rail, and catenary. The connection between the bridge and rail was simulated using a nonlinear connection element, while the catenary was connected to the simply-supported beam through a rigid arm. The simulation model that was established is illustrated in Figure 5.

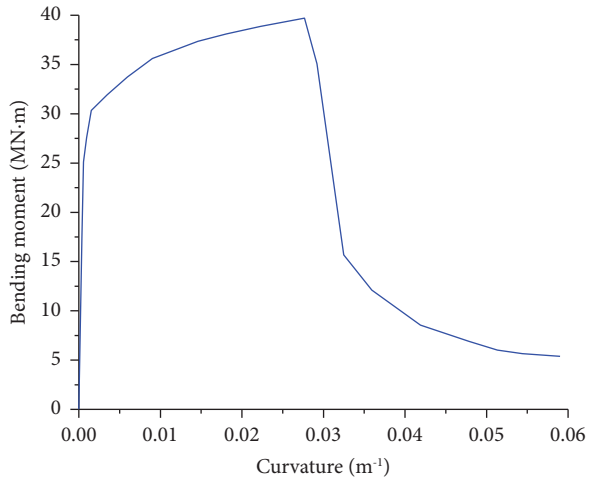

Figure 4: The curve of bending moment-curvature of the pier section.

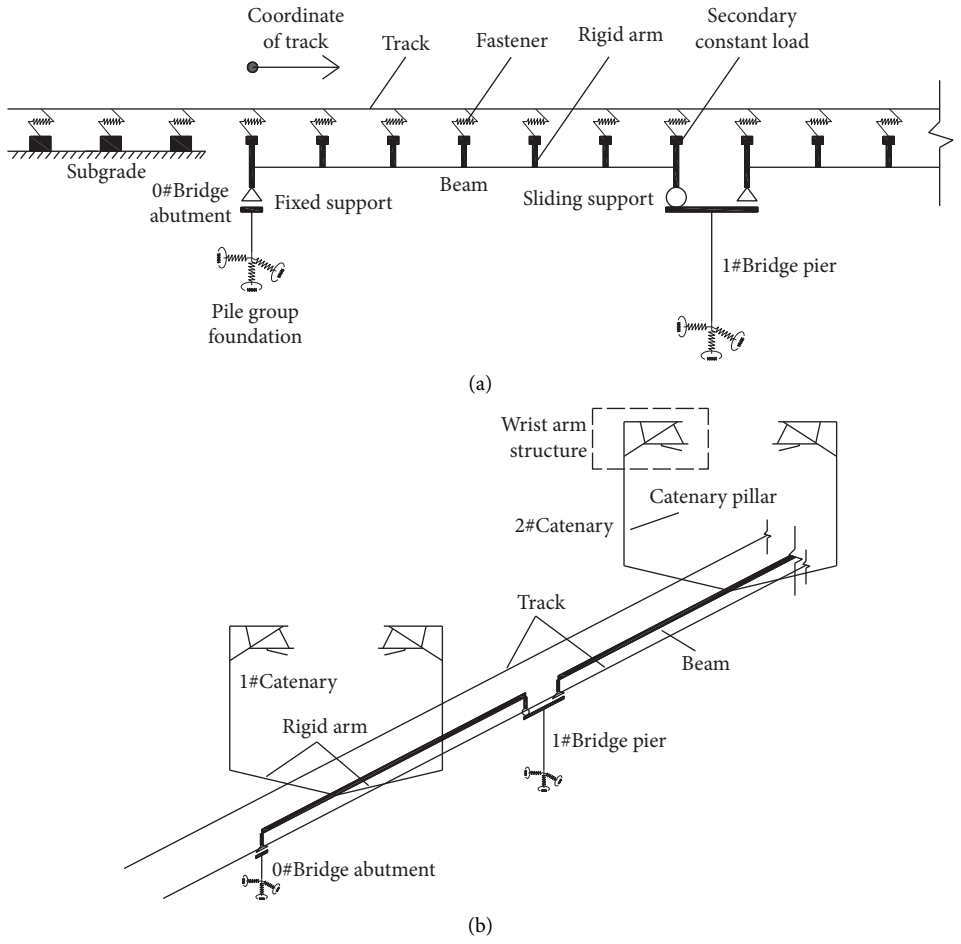

Figure 5: Catenary-bridge-track simulation model. (a) Bridge-track interaction model; (b) bridge-catenary interaction model.

2.2. Setting of the Longitudinal Resistance of the Line. In the finite element simulation model of the catenary-bridge-track system, the longitudinal resistance of the track is typically simulated using an ideal elastoplastic model. In this study, the longitudinal resistance between the rail and bridge was modeled using the longitudinal resistance of ballastless track fasteners, the longitudinal resistance of ballasted track bed, and the longitudinal resistance of small resistance fasteners under no-load condition, as described by formulas (1), (4), and (5) [15]:

$$r_{L_2}\begin{cases} 7.5x, & |x| \le 2.0, \\ 15.0\text{sign}(x), & |x| > 2.0, \end{cases} \tag{4}$$

$$r_{L_3}\begin{cases} 16.0x, & |x| \le 0.5, \\ 8.0\text{sign}(x), & |x| > 0.5, \end{cases} \tag{5}$$

where r_{L_2} is the longitudinal resistance of ballasted track bed, kN/m per line; r_{L_3} is the longitudinal resistance of small resistance fasteners, kN/m per line; and x is the longitudinal displacement of the rail relative to the fastener, mm.

3. Seismic Vulnerability Analysis Based on IDA

3.1. Analysis Method and Earthquake Input. The incremental dynamic analysis (IDA) technique is a seismic evaluation method that accounts for both structural demand and capacity. This approach involves scaling ground motion using a proportional coefficient to generate a range of structural responses at different seismic intensities. Subsequently, a relationship curve between ground motion intensity parameters and structural damage parameters, known as the IDA curve, is plotted. This curve can illustrate the trend of structural response variations with changes in ground motion intensity [18, 19].

Based on pertinent standards and prior research experience, 20 appropriate ground motion records were culled from the seismic record database maintained by the Pacific Earthquake Engineering Research Center [20, 21]. The relevant information of seismic wave is shown in Table 2, and the acceleration response spectra of these records are shown in Figure 6.

The peak ground acceleration (PGA) was selected as the ground motion intensity parameter, and amplitude adjustment treatment of the seismic wave was performed while preserving its spectral characteristics. Specifically, the PGA values of 0.05 g, 0.1 g, 0.2 g, 0.4 g, and 0.8 g were utilized, and the structures were then analyzed using the Newmark-β method for nonlinear time course.

3.2. Establishment of Vulnerability Curves. The probabilistic seismic demand model demonstrates the probabilistic relationship between the seismic demand of a structure and the intensity of ground shaking, thereby laying the groundwork for formulating vulnerability curves.

The probability of failure of a structure, based on seismic demand and ground shaking intensity, can be indicated in the following formula:

$$P_f = P[D \ge C|\text{IM}], \tag{6}$$

where P_f is the probability of failure of the structure; D is structural seismic demand or Engineering Demand Parameters, expressed as the seismic response of a structure, i.e. the structural damage parameters in the IDA method; C is the structural capacity, which corresponds to the damage index of the structure in the vulnerability analysis; and IM is the ground motion intensity parameter in the IDA method, which is used in this study as the PGA.

As per Cornell et al., it is assumed that the mean seismic demand follows an exponential relationship with IM [22], i.e.,

$$S_D = a\text{IM}^b, \tag{7}$$

where S_D is the mean value of the structural seismic demand D and a and b are exponential relationship coefficients.

Formula (8) can be obtained by transforming formula (7) into a logarithmic expression.

$$\ln(S_D) = \ln(a) + b\ln(\text{IM}). \tag{8}$$

Formula (8) represents a linear regression that is fitted to the logarithmic IDA curve. This formula serves as the probabilistic seismic demand model that is necessary for conducting the susceptibility analysis.

As per the conventional theory of structural reliability, a structure is deemed to have failed if the load effect surpasses the resistance of the structure. In the context of seismic susceptibility analysis using the IDA approach, this can be expressed through the following formula:

$$\begin{aligned} P_f &= P\left[\frac{S_D}{S_C} \ge 1\right] \\ &= P\left[\ln\frac{S_D}{S_C} \ge 0\right], \end{aligned} \tag{9}$$

where S_D is the seismic demand of the structure, determined by a probabilistic seismic demand model, and S_C is the load-bearing capacity of the structure, determined by damage index.

It is shown that both S_D and S_C can be considered to obey a log-normal distribution, and then the probability of failure of the structure can be expressed in the following formula [23]:

$$P_f = \Phi\left[\frac{1}{\sqrt{\beta_d^2 + \beta_c^2}}\ln\left(\frac{S_D}{S_C}\right)\right], \tag{10}$$

where $\Phi(\cdot)$ is the standard normal distribution function and β_d and β_c are the standard deviations of the logarithms of S_D and S_C, respectively.

By substituting formulas (8) into (10), the transcendental probability function for the structure can be obtained, as illustrated in the following formula:

$$P_f = \Phi\left[\frac{\ln(a) + b\ln(IM) - \ln(S_C)}{\sqrt{\beta_d^2 + \beta_c^2}}\right]. \tag{11}$$

Since the independent variable IM was used in this study as PGA, $\sqrt{\beta_d^2 + \beta_c^2}$ was taken to be 0.5 [24].

Based on the calculated beyond probability function, the susceptibility curves were established. This study focuses on investigating the vulnerability of the structure by analyzing the fasteners and catenary.

Table 2: Seismic wave information.

Number	Earthquake name	Station name	PGA (g)	Time (s)
RSN6	Imperial Valley-02	El Centro Array #9	0.2540	53.72
RSN9	Borrego	El Centro Array #9	0.0659	50.00
RSN15	Kern County	Taft Lincoln School	0.1590	54.35
RSN17	Southern Calif	San Luis Obispo	0.0497	40.00
RSN28	Parkfield	Cholame-Shandon Array #12	0.0597	44.30
RSN31	Parkfield	Cholame-Shandon Array #8	0.2720	26.21
RSN40	Borrego Mtn	San Onofre-So Cal Edison	0.0413	45.21
RSN55	San Fernando	Buena Vista-Taft	0.0120	26.65
RSN56	San Fernando	Carbon Canyon Aam	0.0710	40.00
RSN59	San Fernando	Cedar Springs Allen Ranch	0.0153	14.74
RSN67	San Fernando	Isabella dam (Aux Abut)	0.0095	42.43
RSN68	San Fernando	LA-Hollywood Stor FF	0.2250	79.45
RSN77	San Fernando	Pacoima Dam (upper left abut)	0.3072	41.72
RSN83	San Fernando	Puddingstone Dam (abutment)	0.0736	32.81
RSN85	San Fernando	San Juan Capistrano	0.0433	98.81
RSN86	San Fernando	San Onofre-So Cal Edison	0.0159	52.47
RSN88	San Fernando	Santa Felita Dam (Outlet)	0.1550	40.00
RSN92	San Fernando	Wheeler Ridge-Ground	0.0260	29.76
RSN93	San Fernando	Whittier Narrows Dam	0.1080	40.00
RSN94	San Fernando	Wrightwood-6074 Park Dr	0.0547	19.96

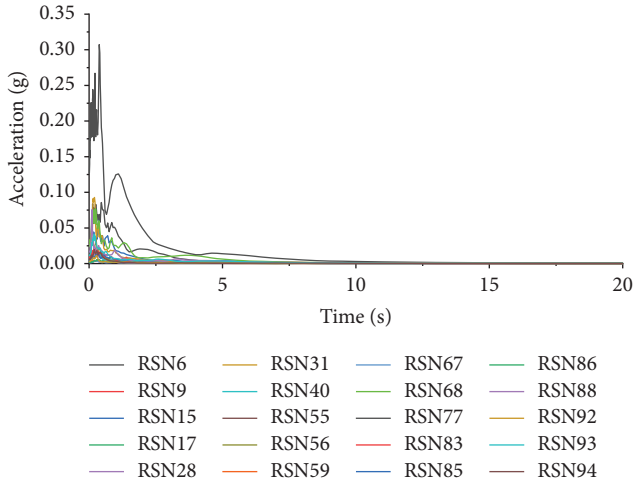

Figure 6: The acceleration response spectrum of seismic wave.

3.3. Vulnerability Analysis of Fasteners. The damage state of the fastener was categorized into five distinct levels, and a quantitative assessment of the deterioration state was achieved by utilizing the deformation-based failure criteria, where the displacement parameter was employed as the damage index [20], as depicted in Table 3.

Fasteners located at the stationary support, middle section, and sliding support of the initial, central (i.e., the fourth), and final (i.e., the seventh) spans of the simply-supported beam were designated as representatives for executing vulnerability analysis. These fasteners were labeled as follows: 1-fixed end, 1-mid-span, 1-sliding end, 4-fixed end, 4-mid-span, 4-sliding end, 7-fixed end, 7-mid-span, and 7-sliding end, correspondingly. Figure 7 presents the vulnerability curves of the fasteners at distinct positions, subjected to varying damage states.

According to Figure 7, within a certain range of seismic intensity, the exceedance probability of fasteners at the same position for a certain damage state increases with the increase of PGA. With the increase of the damage state, the exceedance probability of fasteners at the same position decreases gradually.

The vulnerability curves of fasteners located at the 1-fixed end and 7-sliding end appear to be similar under the same damage state. However, at the same exceedance probability, the PGA of the 7-sliding end is lower, indicating that the vulnerability of fastening elements at both ends of a multispan simply-supported girder bridge for the high-speed railway is significantly influenced by the track structure of the subgrade at both ends. The vulnerability of fasteners at the 1-sliding end is noticeably higher than that at the 7-fixed end, and the discrepancy increases significantly with the augmentation of the damage state, revealing that it is greatly affected by the end fixation of the beam. The vulnerability of fasteners located at 1-mid-span and 7-mid-span is comparable. As the damage state increases, the vulnerability gap gradually increases, indicating that fasteners located at the middle of the span of the simply-supported beam at both ends are affected by the track structure of the subgrade and the fixation of the beam end, and as the damage state increases, the influence of the fixation of the beam end also increases. The vulnerability of fasteners on the central span of the beam is relatively low overall, and the middle part of the span is hardly damaged.

3.4. Vulnerability Analysis of Catenary. This paper accounted for the limit value of the dynamic lift of the catenary [25], and the displacement of the endpoint of the locator at the fixed contact line position was utilized as the damage index to provide a quantitative depiction of the damage state of the catenary, as presented in Table 4.

Table 3: Damage state assessment of fastener (unit: mm).

Damage state	Zero damage	Minor damage	Moderate damage	Severe damage	Complete damage
Displacement	$0 \le d < 2$	$2 \le d < 3$	$3 \le d < 4$	$4 \le d < 5$	$d \ge 5$

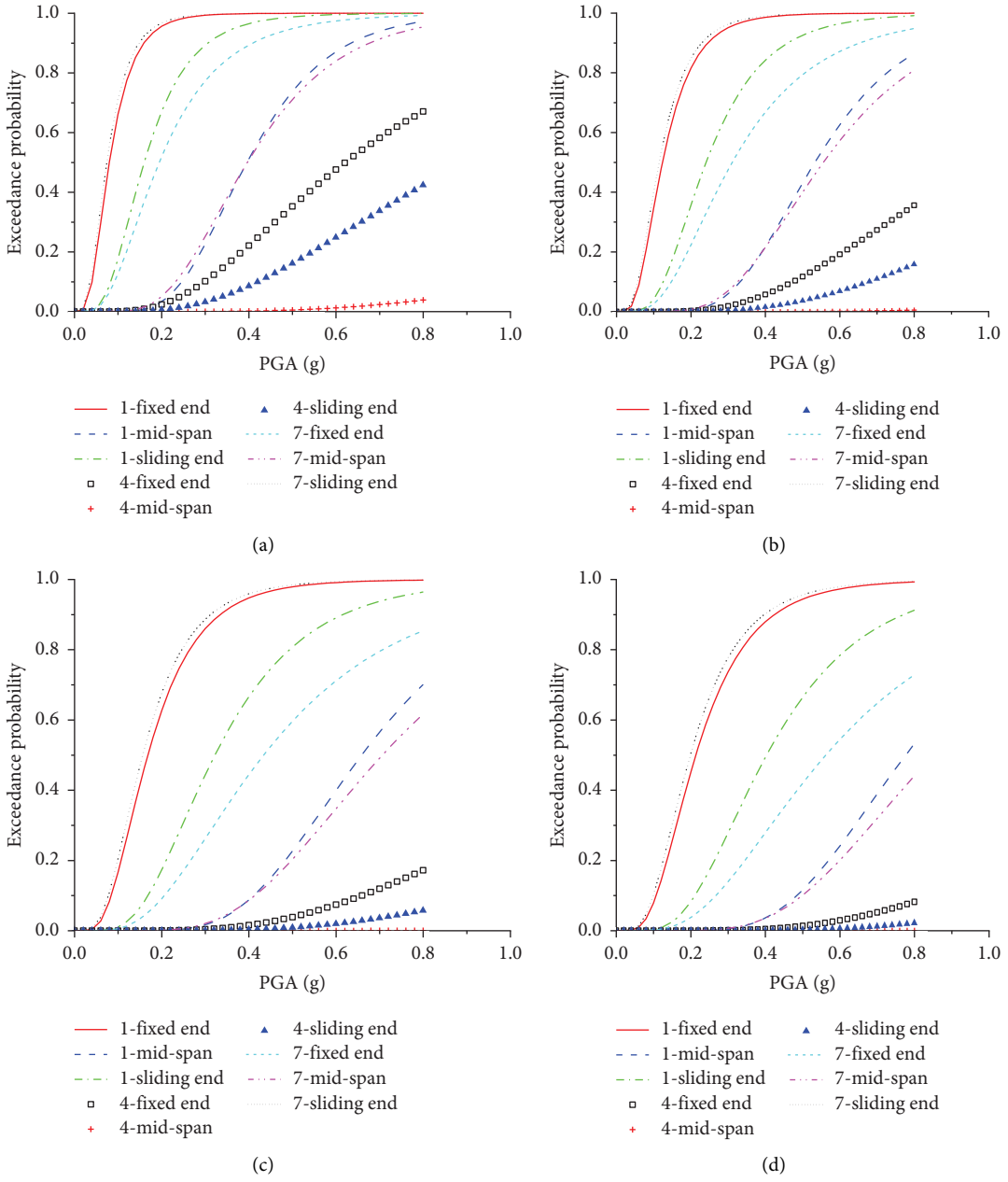

Figure 7: Vulnerability curve of fasteners. (a) Minor damage; (b) moderate damage; (c) severe damage; (d) complete damage.

Table 4: Damage state assessment of catenary (unit: mm).

Damage state	Zero damage	Minor damage	Moderate damage	Severe damage	Complete damage
Displacement	$0 \le D < 30$	$30 \le D < 60$	$60 \le D < 90$	$90 \le D < 120$	$D \ge 120$

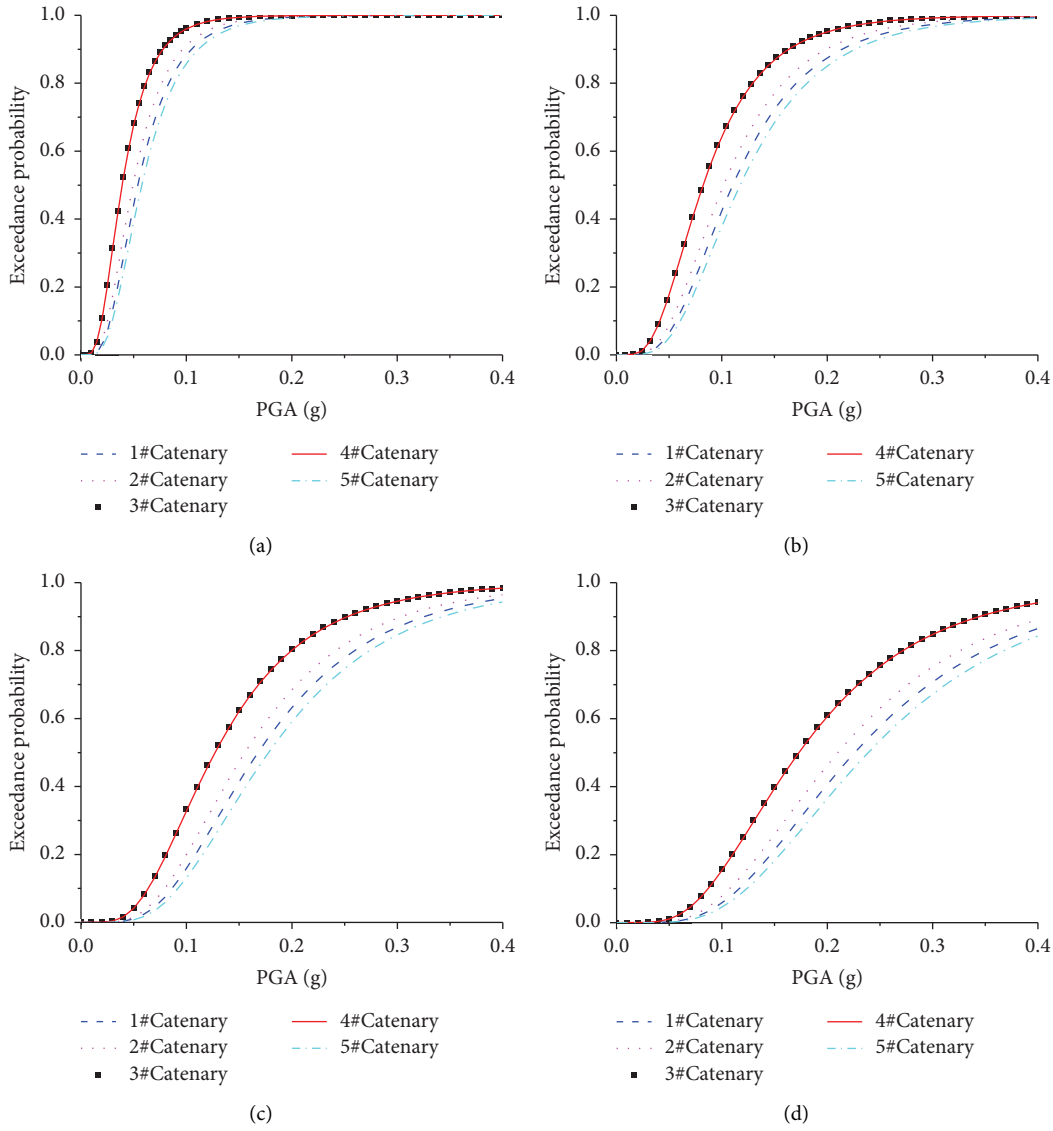

Figure 8: Vulnerability curve of catenary. (a) Minor damage; (b) moderate damage; (c) severe damage; (d) complete damage.

The vulnerability curves of five catenary groups under various damage states are depicted in Figure 8 for the simulation model of the catenary-bridge-track system established in this study.

The exceedance probability of the same catenary for a particular damage state tends to increase within a specific range of seismic intensity as the PGA rises. As the damage state increases, the exceedance probability of the same catenary gradually diminishes.

The exceedance probability of the catenary varies significantly under diverse damage states. When the damage state is relatively small, the vulnerability of each catenary is relatively concentrated. As the damage state increases, the gap in vulnerability between catenaries gradually enlarges. Among all catenaries, the 3# catenary near the middle of the bridge span is the most vulnerable under the same damage state and seismic intensity, whereas the 1# and 5# catenary at the end of the bridge are relatively less vulnerable.

4. Influence of the Longitudinal Resistance of Line on Fastener Vulnerability

Based on the fastener vulnerability analysis, it can be concluded that for a multispan simply-supported girder bridge, fasteners at both ends are more susceptible to damage, and their vulnerability is somewhat similar. Conversely, fasteners on the mid-span have relatively lower vulnerability. In this study, the fastener at the center of the first span of the simply-supported beam was chosen as the representative, and various longitudinal resistances of the line were set to investigate their vulnerability changes, as illustrated in Figure 9.

For the fastener located at the middle of the 1st span of the simply-supported beam, also known as the middle of the side span, its vulnerability is significantly affected by the longitudinal resistance of the line under different damage states. Within a certain range of seismic intensity, the

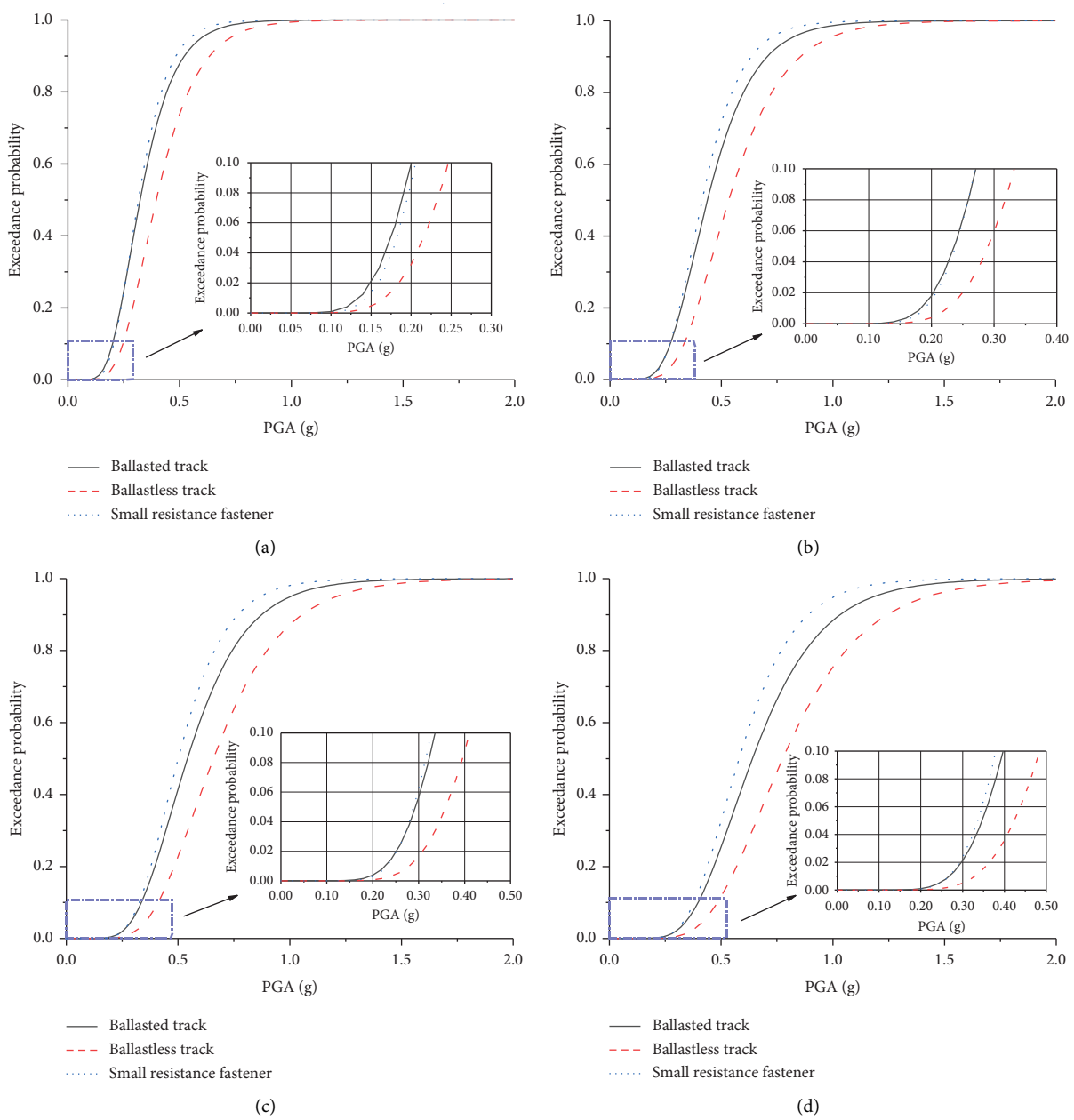

Figure 9: Comparison of fastener vulnerability curve. (a) Minor damage; (b) moderate damage; (c) severe damage; (d) complete damage.

exceedance probability of the small resistance fastener is the highest for a certain damage state, followed by ballasted track, and the lowest for the ballastless track. When the exceedance probability is set to 5%, the failure sequence of fasteners is the ballasted track, small resistance fastener, and ballastless track in order when the damage degree is small. With the increase of the damage state, the small resistance fastener will be damaged before the ballasted track.

5. Influence of the Longitudinal Resistance of Line on Catenary Vulnerability

By analyzing the vulnerability of the catenary, it becomes evident that the vulnerability curves of the catenary on the bridge demonstrate a certain degree of regularity and similarity under different damage conditions. Building upon this foundation, the 3# catenary with the highest degree of vulnerability was chosen as the representative, and various longitudinal resistances of the line were established to investigate the alterations of the catenary's vulnerability. The vulnerability curves are illustrated in Figure 10.

Under different damage states, the vulnerability curves of 3# catenary remain relatively similar across different longitudinal resistances of the line, suggesting minimal impact of longitudinal resistance on catenary vulnerability. Taking the exceedance probability of 5% as the criterion, catenary failure occurs in the order of ballastless track, ballasted track, and small resistance fastener. It is

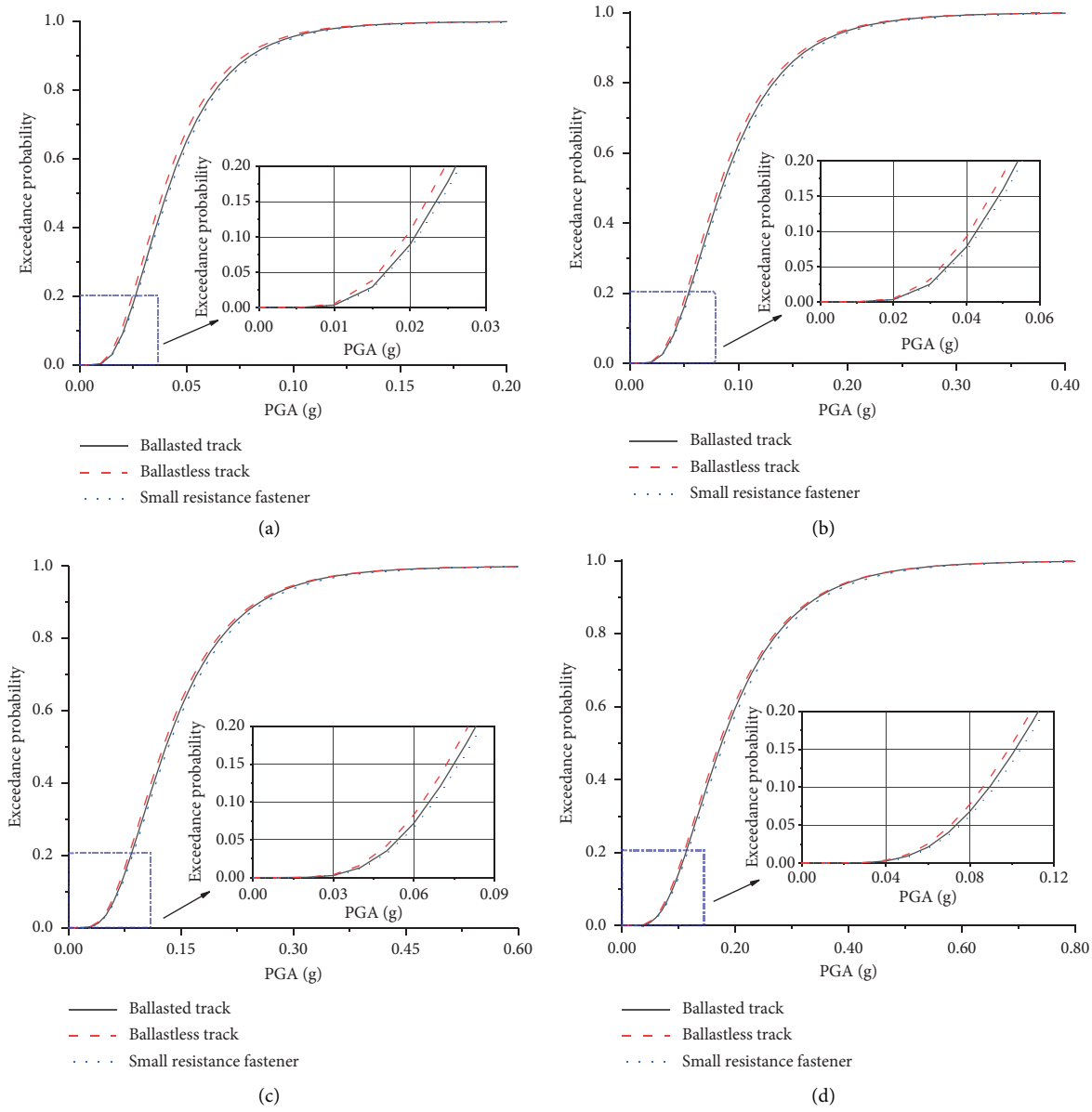

Figure 10: Comparison of catenary vulnerability curve. (a) Minor damage; (b) moderate damage; (c) severe damage; (d) complete damage.

noteworthy that the catenary of ballastless track proves to be more sensitive to ground motion.

6. Structural Response under Ground Motion

Taking into account the seismic fortification intensity of 8 degrees and a PGA value of 0.3 g, the probabilities of 1-mid-span fastener and 3# catenary reaching different damage states under various longitudinal resistances of the line were calculated, as presented in Figure 11.

As depicted in Figure 11(a), at a PGA of 0.3 g, the probability of damage for the fastener at the 1-mid-span position is at its highest in the undamaged state. The ballastless track significantly improves the probability of no damage to fasteners, ensuring safety of fasteners. Similarly, the exceedance probability of ballasted track and small resistance fastener is relatively similar under the same damage state, indicating that the effect of these two track structures on fastener damage states is negligible.

As shown in Figure 11(b), 3# catenary is unable to remain undamaged when PGA is 0.3 g. There is minimal variation in the exceedance probability of the three track structures under different damage states. The longitudinal resistance of the line has only a minor effect on the probability of different damage states occurring in the 3# catenary. In terms of complete damage, the ballastless track has the highest probability of exceeding, followed by ballasted track, and the small resistance fastener track has the lowest probability of exceeding, with probabilities of 85.0%, 84.4%, and 83.1%, respectively.

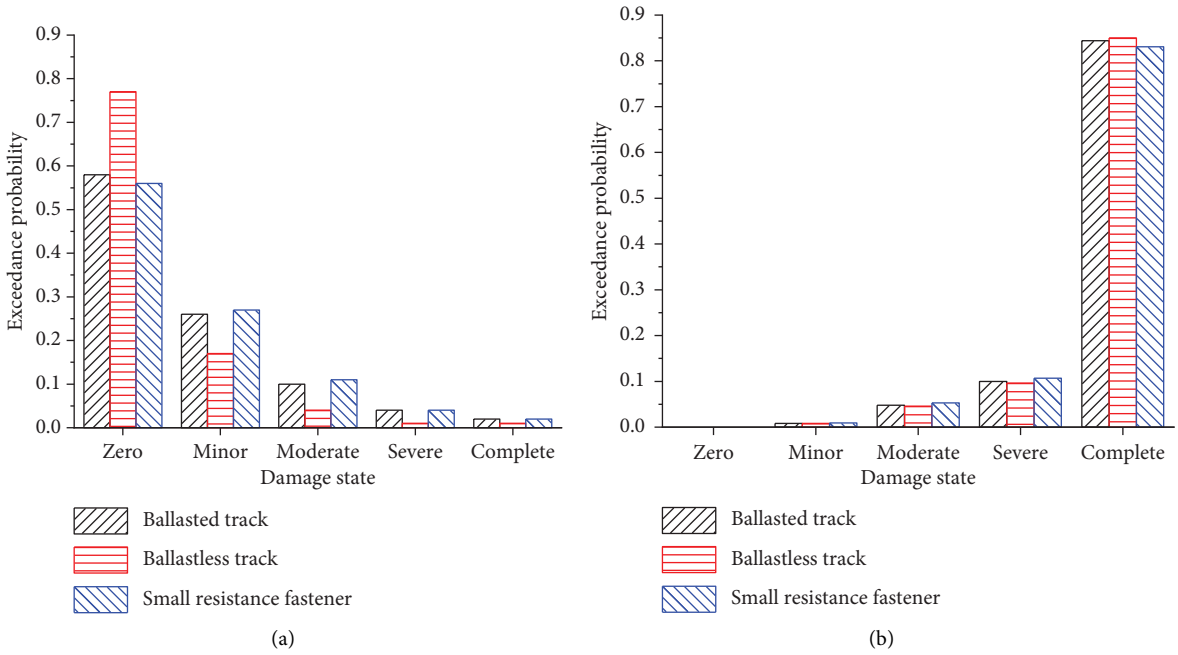

Figure 11: Probability of different damage states (PGA = 0.3 g): (a) Mid-span fastener; (b) 3# catenary.

7. Conclusions

To examine the impact of longitudinal resistance on the vulnerability of the catenary-bridge-track system, a sophisticated simulation model of a 7–32 m simply-supported beam bridge system was constructed, taking into account various components such as the catenary pillar, wrist arm structure, steel rail, fastener, beam, support, bridge pier, bridge abutment, and pile group foundation. Using the IDA method, this study revealed the damage pattern of fasteners and catenary on high-speed railway bridges under seismic conditions, along with the influence of longitudinal resistance on fasteners and catenary. The primary findings of this study are as follows:

(1) Within a certain range of seismic intensity, the probability of fasteners and catenary on the bridge reaching a specific damage state increases as the ground motion intensity increases. When PGA reaches a certain threshold and the exceedance probability approaches 1, the structure is considered to be damaged. Catenary is found to be more vulnerable to earthquakes compared to fasteners.

(2) The vulnerability of fasteners located near the abutments at both ends of multispan simply-supported beam bridges is greatly affected by the track structure of the subgrade, whereas those near the middle of the side span display similar vulnerability. In contrast, the fasteners located at the mid-span exhibit minimal damage. In addition, the vulnerability of fasteners located in the middle of each span is considerably lower than those located at the fixed and sliding ends.

(3) The exceedance probability of each catenary exhibits a significant variation under distinct damage states, and the gap in vulnerability between catenaries widens as the damage state increases. Under the same damage and seismic intensity, the 3# catenary positioned close to the bridge's center displays the highest vulnerability, while the catenaries situated at both ends of the bridge exhibit a relatively lower vulnerability.

(4) The longitudinal resistance of the line exerts a greater influence on the vulnerability of fasteners than on that of the catenary. When using a 5% exceedance probability as a benchmark for small damage states, the failure order of fasteners is ballasted track, small resistance fastener, and ballastless track. As the damage degree increases, the small resistance fastener will fail before the ballasted track. For the catenary, the damage sequence is the ballastless track, ballasted track, and small resistance fastener.

(5) At a peak ground acceleration of 0.3 g, the probability of no damage to the 1-mid-span fastener is highest, while the probability of complete damage to the 3# catenary is maximum. The ballastless track structure obviously improves the probability of no damage to the 1-mid-span fastener, and the longitudinal resistance of the line has little impact on the 3# catenary.

Data Availability

The data used to support the findings of this study are included within the article.

Conflicts of Interest

The authors declare that they have no conflicts of interest.

Acknowledgments

This research was funded by the National Natural Science Foundation of China (Project no. 52278470) and the Natural Science Foundation of Hunan Province (grant no. 2022JJ30741).

References

[1] H. T. Qian, *Research on Seismic Responses and Seismic Fragility Analysis of Continuous Welded Rails on Simply-Supported Bridge*, Southwest Jiaotong University, Sichuan, China, 2018.

[2] L. Q. Wu, *Research and Application on the Detection of Geometric Parameters of Catenary*, China Academy of Railway Sciences, Beijing, China, 2020.

[3] D. H. Tavares, J. R. Suescun, P. Paultre, and J. E. Padgett, "Seismic fragility of a highway bridge in quebec," *Journal of Bridge Engineering*, vol. 18, no. 11, pp. 1131–1139, 2013.

[4] C. S. W. Yang, S. D. Werner, and R. Desroches, "Seismic fragility analysis of skewed bridges in the central southeastern United States," *Engineering Structures*, vol. 83, pp. 116–128, 2015.

[5] G. H. Siqueira, A. S. Sanda, P. Paultre, and J. E. Padgett, "Fragility curves for isolated bridges in eastern Canada using experimental results," *Engineering Structures*, vol. 74, pp. 311–324, 2014.

[6] L. F. Li, W. P. Wu, and J. M. Huang, "Study on system vulnerability of medium span reinforced concrete continuous girder bridge under earthquake excitation," *China Civil Engineering Journal*, vol. 45, pp. 152–160, 2012.

[7] P. Yang and G. J. Yang, "Analysis of seismic vulnerability and adaptation of simply-supported girder bridge on sichuan-tibet railway," *Journal of Railway Engineering Society*, vol. 32, pp. 51–57+75, 2015.

[8] S. Song, Y. J. Qian, and G. Wu, "Mixed copula function method for seismic fragility analysis of bridge system," *Engineering Mechanics*, vol. 34, pp. 219–227, 2017.

[9] J. Dong, Y. P. Zeng, and D. S. Shan, "Three-dimensional seismic vulnerability analysis of long-span railway bridge components with high pier," *Journal of Harbin Institute of Technology*, vol. 51, pp. 141–149, 2019.

[10] M. Kim, Y. Park, S. R. Han, and S. Choi, "Earthquake response characteristics of the catenary Pole for arrangement conditions," *Journal of The Korean Society of Hazard Mitigation*, vol. 18, no. 3, pp. 31–36, 2018.

[11] S. Gregori, J. Gil, M. Tur, J. E. Tarancon, and F. J. Fuenmayor, "Analysis of the overlap section in a high-speed railway catenary by means of numerical simulations," *Engineering Structures*, vol. 221, Article ID 110963, 2020.

[12] Y. Liu, W. H. Zhang, and B. Huang, "Experiment and simulation of dynamic response of high-speed railway catenary," *China Railway Science*, pp. 109–112, 2005.

[13] J. Zhang and Q. Xie, "Analysis of seismic response of high-speed railway catenary system," *Railway Standard Design*, vol. 61, pp. 140–146, 2017.

[14] Q. Zhang, H. M. Li, M. A. Li, Y. Xuan, and W. A. N. Jia, "Safety threshold of catenary system on high-speed railway bridge under earthquake condition," *China Railway Science*, vol. 37, pp. 64–69, 2016.

[15] China Railway Publishing Home, *TB10015-2012 Code for Design of Railway Continuously Welded Rail*, China Railway Publishing Home, Beijing, China, 2013.

[16] UIC 774-3.Track/Bridge Interaction, *Recommendations for Calculations*, International Union of Railways, Paris, 2001.

[17] B. Yan, S. Liu, G. L. Dai, H. Pu, and J. Tang, "Nonlinear interaction between CRTS II ballastless track and bridges due to multi-dimensional earthquake," *Journal of the China Railway Society*, vol. 38, pp. 74–80, 2016.

[18] M. Z. Cui, C. H. Chen, C. K. Wang, Y. H. Pan, and Y. H. Xiong, "Seismic fragility analysis on existing high-rise shear-wall structure based on incremental dynamic analysis," *Building Science*, vol. 37, pp. 151–157, 2021.

[19] D. Vamvatsikos and C. A. Cornell, "Incremental dynamic analysis," *Earthquake Engineering & Structural Dynamics*, vol. 31, no. 3, pp. 491–514, 2002.

[20] B. Wei, C. J. Zuo, X. H. He, and L. Z. Jiang, "Effects of vertical ground motions on seismic vulnerabilities of a continuous track-bridge system of high-speed railway," *Soil Dynamics and Earthquake Engineering*, vol. 115, pp. 281–290, 2018.

[21] GB 50111-2006, *Code for Seismic Design of Railway Engineering*, China Planning Press, Beijng, China, 2009.

[22] C. A. Cornell, F. Jalayer, R. O. Hamburger, and D. A. Foutch, "Probabilistic basis for 2000 SAC federal emergency management agency steel moment frame guidelines," *Journal of Structural Engineering*, vol. 128, no. 4, pp. 526–533, 2002.

[23] L. Q. Wu, *Research and Application on the Detection of Geometric Parameters of Catenary*, Hebei University of Engineering, Hebei, China, 2021.

[24] H. Hwang and J. B. Liu, "Seismic fragility analysis of reinforced concrete bridges," *China Civil Engineering Journal*, vol. 38, pp. 47–51, 2004.

[25] Q. Zhang, *Research and Application on the Detection of Geometric Parameters of Catenary*, China Academy of Railway Sciences, Beijing, China, 2014.